Journal of Artificial Intelligence in Medical Applications (JAIMA)
Vol. 1, No. 1, 2025, **pp**. 15–27
**ISSN**: 3106-1494 | **DOI**: https://doi.org/10.65511/jaima.v1i1.736

# A Robust Colour-Based Framework for Automated White Blood Cells Segmentation Using an Optimised HSV Thresholding via Differential Evolution Approach

**Shumoos Al-Fahdawi [1, *] Alaa S. Al-Waisy [2], and Rami Qahwaji [3]**
[1] Department of Computer Science - College of Computer Science and Information Technology, University of Anbar, Anbar Province, Iraq; shumoos.alfahdawi@uoanbar.edu.iq
[2] Electronic Computer Center, University of Anbar, Anbar Province, 31001, Iraq; alaa.alwaisy@uoanbar.edu.iq
[3] Faculty of Engineering and Digital Technologies, University of Bradford, BD7 1DP Bradford, U.K; R.S.R.Qahwaji@bradford.ac.uk

*Received: 28/05/2025, Revised: 11/07/2025, Accepted: 23/07/2025, Published: 16/09/2025*

**ABSTRACT**: Accurate segmentation of white blood cells (WBCs) in microscopic blood smear images is critical for diagnosing haematological disorders such as leukemia. However, manual analysis by pathologists remains labor-intensive and prone to variability, necessitating automated solutions. This study proposes a color-based WBCs segmentation framework leveraging the HSV color space and Differential Evolution (DE) optimization approach to address challenges posed by heterogeneous staining, overlapping cells, and imaging artefacts. The proposed WBCs segmentation framework operates in three stages: pre-processing via contrast enhancement and HSV transformation, region-based segmentation using DE-optimized dual-thresholding, and post-processing with morphological operations. The DE approach can learn to adaptively determine best-fit HSV thresholds for the separation of WBCs without heavy dependence on annotated datasets or deep learning architectures. Experimental analysis on the BCCD and ALL-IDB2 datasets demonstrates superior performance, with IoU scores of 99.56% and 98.78%, Dice coefficients of 97.23% and 99.53%, and F1-scores of 99.44% and 99.18%, respectively. By combining stochastic optimization with color space analysis, the presented framework yields a computationally efficient, interpretable alternative to complex deep learning models, enabling robust WBCs segmentation in resource-constrained clinical environments. The study refers to the potential of the proposed framework for incorporation into computer-automated diagnostic systems, which would minimize the dependence on manual analysis and enhance diagnostic throughput and consistency.

***Keywords:*** Region-based segmentation, White blood cells segmentation, Differential Evolution, BCCD dataset, ALL-IDB2 dataset, Stochastic optimization.

## 1. INTRODUCTION

Blood is essential for life sustenance in the human body. It consists of two primary components: blood cells and plasma. Plasma, a light yellowish fluid, constitutes approximately 55% of the total blood volume [1]. Besides plasma, blood also includes various components like blood cells, hormones, carbon dioxide, proteins, carbohydrates, and small amounts of nutrients. The major cellular components of blood are red blood cells (RBCs), WBCs, and platelets (thrombocytes), which are distinguished by their morphology and structural characteristics [2]. Within the WBC category, there are five main categories: neutrophils, eosinophils, basophils, monocytes, and lymphocytes. WBC classification is an important part of haematological imaging for the identification and diagnosis of a wide range of diseases, such as leukemia, various types of cancers, and certain immunological diseases [3]. For clinical practice, WBCs are examined from samples drawn from peripheral blood smears or bone marrow. Samples are stained and prepared for examination under the microscope using a process of slide mounting and differential staining techniques, which provide characteristic color patterns for cell components such as nuclei, cytoplasm, plasma, and RBCs [4]. In clinical settings, detection, segmentation, and counting of WBCs in these images have been performed manually by specialists, which is a time-consuming process requiring lots of effort [5]. Therefore, there is a demand for a robust and fully automated method of WBC segmentation to render diagnostic, treatment, and therapeutic procedures more efficient and streamlined. Complete automatic segmentation of WBCs, nevertheless, is confronted by several challenges. One of these major challenges is the fact that cytopathological image datasets are typically gathered from various sources in hospitals, using different devices, and under different lighting and staining conditions. In addition, manual intervention in the preparation of cell smears or tissue sections introduces variations such as cell deformation, blurred cell borders, and cell color heterogeneity. Besides, cytopathological images are usually composed of numerous cells with a large variety of complicated shapes and structures, offering high variability in shape and size. Such a complex nature usually leads to overlapping or adherent cells, which further generate challenges in accurate segmentation. So far, accurate segmentation of WBCs remains an open problem, still attracting considerable attention and encouraging the invention of automated image analysis techniques.

This paper presents a color-space segmentation approach to WBC segmentation in three main stages: image pre-processing, region-based segmentation, and image post-processing. During the image pre-processing stage, two improved images are generated, one by mapping a sigmoid function to improve contrast, and the

other transformed into the HSV color space to obtain prominent color features for WBC detection. The region-based segmentation stage begins with the elimination of the background, using Adaptive Gaussian Thresholding (AGT) and morphological processing of the contrast-stretched image, making it more adaptable to varying light conditions. For WBC extraction, dual-thresholding of the HSV image is done using thresholds optimized using the DE optimization technique. The stochastic optimization enhances performance with changing imaging conditions. Lastly, during the image post-processing stage, morphological closing and connected components analysis are utilized to remove noise without disturbing the white blood cells' contour integrity. These stages collectively constitute an entire, multi-stage algorithm that drastically improves white blood cell segmentation in intricate blood smear images. The key contributions of this research can be summarized as follows:

1. A robust, color-based framework was presented for WBC segmentation in difficult microscopic images. By combining contrast enhancement techniques with HSV color space analysis, the developed framework effectively separates WBCs from background material and adjacent cells, counteracting problems like overlapping structures and non-uniform staining.
2. The key innovation includes the application of a dual-thresholding technique to HSV channels using optimum threshold values determined by the DE optimization approach. The stochastic optimization approach fosters adaptability to varying image conditions, optimizing threshold calculation, significantly improving segmentation accuracy without reliance on massive, annotated datasets (training data) or deep learning approaches.
3. The suggested segmentation pipeline is organized into three clearly defined phases: image pre-processing, region-based segmentation, and image post-processing. Each phase is meticulously crafted to progressively improve image quality, delineate regions of interest, and refine segmented outputs through morphological operations and connected components analysis for structural intactness and noise removal.
4. With the inclusion of AGT for background elimination and DE-based optimized thresholding for WBCs segmentation, the proposed framework is extremely resilient to staining, illumination, and image resolution inconsistencies commonly encountered in real-world medical data sets. This makes the proposed framework very appropriate for applications in automated diagnostic systems in heterogeneous clinical setups.

The organization of the paper is as follows: Section 2 outlines the related research works on WBCs segmentation. Section 3 explains the suggested algorithm for WBCs segmentation. Section 4 introduces the datasets, evaluation measures, and experimental results. Section 5 outlines the conclusions and suggests future work directions.

## 2. RELATED WORKS

Segmentation of WBCs is crucial for the accurate diagnosis of various medical disorders. Recent advances in colour space conversion and thresholding techniques have significantly improved the efficiency of this process. Various approaches exist that employ various colour models such as RGB, Lab, HSV, and CMYK to achieve higher accuracy in segmentation. In addition, the application of deep learning coupled with optimisation techniques has played an important role in further improving these segmentation approaches. As an example, Biswas and Bhattacharya [4] proposed a segmentation method for WBCs through conversion of RGB images to the CMYK colour model, followed by contrast stretching of the M channel. Thresholding and morphological processing were then used to segment areas of interest with WBCs and their cytoplasm. The method was tested on a dataset of 200 images of bone marrow slides, and the quality of segmentation was compared with manually annotated ground truth through the Intersection over Union (IoU) metric. The new technique had a mean IoU of 0.85 (85%) over the dataset. Zang et al. [6] proposed an improved segmentation technique using the segment anything model (SAM). The method starts with preprocessing through contrast-limited adaptive histogram equalisation (CLAHE) for improving the visual quality of WBCs. Then, the application of SAM is employed for precise segmentation. Experimental evaluation indicates that the new method achieves better performance on cross-domain datasets, achieving precise and stable segmentation of WBCs and state-of-the-art performance in the F1 measure and IoU metric. Deshpande et al. [7] suggested a strong segmentation technique for leukaemia identification based on microscopic images from the ALL-IDB dataset. The method integrates Otsu's intensity-based thresholding and Kapur's entropy-based thresholding method with LebTLBO optimisation for the optimisation of the threshold value selection, especially in cases with small histogram variation. The comparison with the Dice score and Jaccard index showed that the optimized Otsu algorithm performed better than its variants, with a Dice score of 0.6325 and a Jaccard index of 0.4723, thereby having greater segmentation accuracy. Deshpande et al. [8] proposed a U-Net-based approach for WBC image segmentation, combining residual blocks and attention mechanisms. For the issue of sparse labeled data, they employed transfer learning using pre-trained ResNet50 on ImageNet as the encoder. Additionally, an SE (Squeeze-and-Excitation) module was added in the decoder for enhancing segmentation accuracy. The method achieved superior performance on

BCISC and LISC datasets with Dice of 98.13%, mIOU of 96.36%, sensitivity of 98.06%, PPV of 98.23%, and Hausdorff Distance of 3.52 on BCISC, and Dice of 95.31%, mIOU of 91.09%, sensitivity of 94.99%, and HD of 4.97% on LISC. Similarly, Resendiz et al. [9] suggested an Explainable AI (XAI) approach to classify leukaemia with a strong WBC nuclei segmentation method as a hard attention mechanism. The segmentation consists of an image processing-based method combined with a U-Net-based structure, which enhances overall performance. These segmented images are further inputted into a modified ResNet-50 structure, including modification of the MLP classifier, activation functions, and training procedure, for the classification of leukaemia subtypes. For interpretability enhancement, visual explanation methods and feature analysis methods were incorporated. The segmentation method achieved a high IoU score of 0.91 in six datasets. Abrol et al. [10] introduced a reliable method combining colour thresholding, marker-based watershed segmentation, and leukocyte localisation. The approach uses peak local maxima to identify leukocytes, generate mask regions, and apply bounding boxes for subsequent analysis. A comparative evaluation was conducted across HSV, YCbCr, and HLS colour spaces to assess blast cell segmentation performance on diverse datasets varying in colour tone, resolution, and magnification. While all three colour spaces achieved an average precision of 94%, HSV demonstrated superior SSIM and recall values compared to the others. Inspired by the YOLACT instance segmentation framework and tailored for cytopathological image characteristics, Luo et al. [11] introduced YOLACT-CIS, a specialised model for WBCs segmentation. The architecture incorporates a Ghost module to reduce network complexity and computational demand. Additionally, a novel DFFN is proposed, introducing a bottom-up pathway in the FPN fusion layer to enhance feature detail capture. Furthermore, the DDAM module is designed to extract global features from both spatial and frequency domains simultaneously, improving overall feature representation. Evaluated on the ALL-IDB and BCCD datasets, YOLACT-CIS achieved superior performance over existing methods such as Mask R-CNN, PointRend, MS R-CNN, SOLOv2, and YOLACT, with an average precision of 87.41%, while significantly lowering model parameters and computational cost.

In spite of the progress in WBCs segmentation techniques reported throughout these studies, there exists a number of limitations. Although some techniques report good performance on individual datasets, their performance, when evaluated with commonly used metrics such as the Dice coefficient and Jaccard index, is short of satisfactory, highlighting the requirement for improvement in segmentation accuracy and robustness. In addition, some of the high-performing deep learning models come with increased architectural and computational cost, which renders them less suitable for deployment in resource-constrained or real-time setups. Others depend to a large extent on transfer learning or data augmentation to compensate for limited annotated data, which may not always be assured of strong generalisation. Finally, while some research incorporates optimisation or explainability techniques, they often lack adequate evaluation on varied or clinically applicable datasets, thus reducing their viability for real-world application. To alleviate these limitations found in existing WBCs segmentation techniques, a colour analysis-based framework is presented that combines a dual-threshold technique with a DE optimisation technique. This framework reduces the reliance of sophisticated deep learning models on huge training data through adaptive thresholding under the DE optimisation technique's guidance, improving robustness across varying imaging conditions. The DE optimisation technique optimises the thresholding, improving accuracy without a heavy computational burden. Its region-based approach allows precise WBC segmentation without requiring large annotated training data, reducing the reliance on large datasets. Thus, the novel WBCs segmentation framework offers efficient, accurate segmentation that can be used in diverse and resource-poor settings.

## 3. THE PROPOSED WBCS SEGMENTATION FRAMEWORK

As shown in Figure 1, the developed segmentation framework of color WBCs is composed of three primary stages: image pre-processing, region-based segmentation, and image post-processing. During the image pre-processing stage, two important images are created for subsequent analysis: one is created with improved contrast to allow visual distinguishability of cellular elements by using a sigmoid function, and the other image is obtained by converting the original image to the Hue, Saturation, and Value (HSV) color space. These images are crucial for improving segmentation accuracy by leveraging color information specific to WBCs. The region-based segmentation stage is composed of two sequential steps: the background removal and the WBCs extraction. In the background removal process, an application of AGT method along with morphological filter operations (Erosion and Dilation) is implemented on the enhanced image produced from the sigmoid function to delineate the region of interest from the background and thus give a better performance under changing lighting conditions compared to global thresholding. In the WBCs extraction step, a dual-thresholding method is applied on the HSV image, which allows WBCs detection according to their distinct color characteristics. In this study, the DE, as a population-driven stochastic optimization approach, is employed to identify the most effective threshold values for extracting WBCs. This approach facilitates precise and adaptable segmentation of WBCs, accommodating the variability present in different imaging conditions. Finally, in the image post-processing stage, a morphological closing operation and

connected components analysis are applied to smooth the segmented areas, eliminate small artefacts, and restore the integrity of the WBCs structures. This multi-stage image segmentation framework improves segmentation performance, making it reliable and efficient for automated detection of WBCs in complex microscopic blood images.

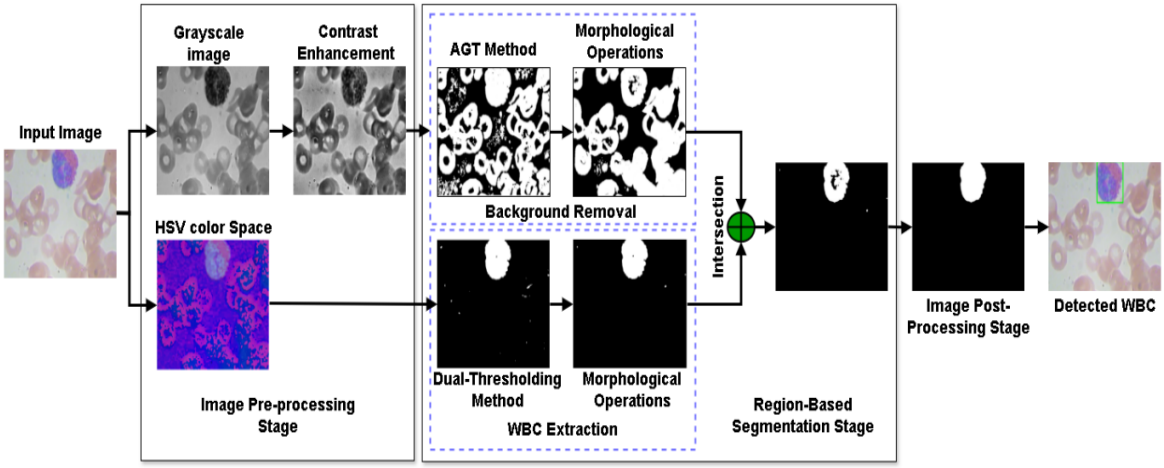


Figure 1: Block diagram of the proposed color-based WBCs segmentation framework.

### 3.1. Image Pre-processing Stage

In this stage, two central images are created for further processing. Initially, the original color image is converted into a grayscale image $\boldsymbol{I_{gray}(x,y)}$, and then the other image is created from transforming the original image into the HSV color space. As shown in the (See Figure 2-b), it is clear that the difference between foreground and background pixels in the grayscale image is typically not adequate to classify the pixels successfully. In order to stretch the dark and light areas of the grayscale image, the sigmoid function is used. It helps to minimize the effect of changes in light by stretching the dark pixels and packing the bright pixels in the grayscale image. The sigmoid function is applied to the $\boldsymbol{I_{gray}(x,y)}$ Image as follows:

$$g(x,y) = \frac{1}{1 + e^{\left(c*\left(Th - I_{gray}(x,y)\right)\right)}} \quad (1)$$

Here, the enhanced image is denoted as $\boldsymbol{g(x,y)}$ and the contrast factor ($\boldsymbol{c}$) was set to **4**, and the threshold value ($\boldsymbol{Th}$) was fixed at **0.5**. These values were selected based on preliminary experiments aimed at achieving a balance between noise suppression and feature preservation, which are critical for accurate segmentation in medical image analysis (See Figure 2-c).

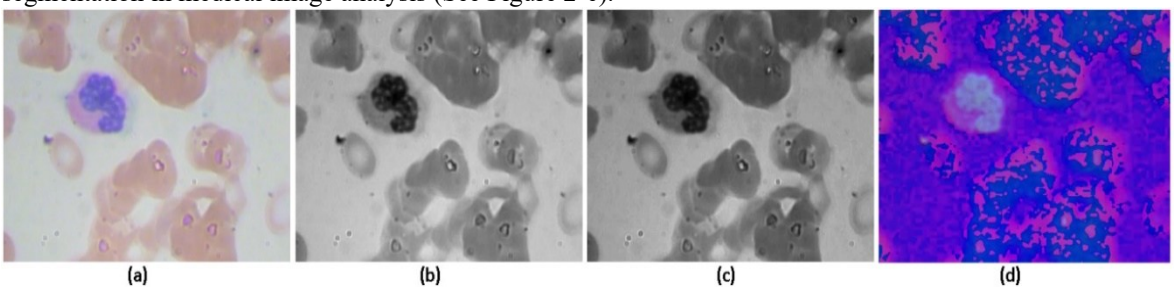


Figure 2: The outputs of the image pre-processing stage: (a) original image, (b) Grayscale image, (c) Enhanced image contrast, and (d) HSV composite.

Conversely, to understand the depiction of HSV channels in the RGB color model, one has to analyze the mathematical interrelations in the geometrical framework of RGB coordinates. This section analyses the conditions in which Hue and Saturation preserve their invariance despite the variations in the values of the RGB components. The ensuing analysis describes the geometrical illustration of Value (brightness) in the boundaries of the RGB cube. Based on this understanding, it becomes feasible to define a projection method that effectively removes or suppresses Value-related information while preserving the chromatic components (e.g., Hue and Saturation). This technique is particularly valuable in applications such as medical image segmentation, including the detection and classification of WBCs, where consistent color representation independent of illumination variations is crucial (See Figure 2- d). RGB vectors are often converted to HSV space as follows:

$$R, G, B \in [0,1]; \quad MAX := max(R, G, B); \; MIN := min(R, G, B)$$

$$H := \begin{cases} 0, & if\ R = G = B \\ 60° * \left(0 + \dfrac{G - B}{MAX - MIN}\right), & if\ MAX = R \\ 60° * \left(2 + \dfrac{B - R}{MAX - MIN}\right), & if\ MAX = G \\ 60° * \left(4 + \dfrac{R - G}{MAX - MIN}\right), & if\ MAX = B \end{cases} \tag{2}$$

$$S := \begin{cases} 0, & if\ R = G = B \\ \dfrac{MAX - MIN}{MAX}, & else \end{cases} \tag{3}$$

$$V := MAX \tag{4}$$

### 3.2. Region-Based Segmentation Stage

The segmentation of WBCs and their nuclei plays a crucial role in classification, counting, and the diagnosis and grading of cancers. The morphology of WBCs and their nuclear structure is often indicative of disease presence and progression. Additionally, cytoplasm segmentation has drawn significant research interest due to its relevance in assessing muscular tissue function and health. However, there remains a shortage of effective computational techniques for analyzing cytoplasm, especially along the longitudinal axis of muscle fibres as most existing studies focus on cross-sectional views or nuclear features. Over the years, various approaches have been developed and combined with other methodologies to improve the detection and segmentation of WBCs, including their nucleus and cytoplasm. In this stage, an efficient and fast region-based segmentation algorithm is developed, consisting of two main steps: background removal and WBCs extraction. Following the application of the sigmoid function, the background exhibits sufficient contrast relative to other image components, enabling its extraction via a single-threshold approach. Nevertheless, as previously noted, achieving complete segmentation of WBCs, encompassing both nuclear and cytoplasmic regions, remains challenging due to the comparable grayscale intensity of cytoplasm and RBCs. Consequently, the initial phase of the proposed region-based segmentation framework focuses on isolating the background regions depicted in black within Figure 2. The background removal step employs AGT method combined with morphological operations, including the Erosion and Dilation operations using the same structure element of size (5×5) on the enhanced image, allowing for robust extraction of the region of interest under varying lighting conditions. In the step of extracting WBCs, a dual-thresholding method is applied to the HSV color image, enabling the detection of WBCs based on their unique color properties. The dual thresholding approach is an image segmentation technique that employs two distinct threshold values (lower and upper thresholds) to more effectively distinguish foreground elements from background or noise. This approach is particularly useful for preserving significant structures that are higher than the upper threshold, while minimizing noise characteristics that are lower than the lower threshold. It also provides selective inclusion of intensity levels of intermediate values based on their spatial relationships or connectivity within the image. When dealing with the HSV color space, one can apply thresholding individually to the Hue (H) component, Saturation (S) component, and Value (V) component to isolate specific ranges of color or particular intensity values. Given an HSV image $\boldsymbol{I_{HSV}(x, y)} = (\boldsymbol{H(x, y)}, \boldsymbol{S(x, y)}, \boldsymbol{V(x, y)})$, the values of lower and upper thresholds for each channel can be defined as follows:

$$T_{low} = (H_{low}, S_{low}, V_{low}), \qquad T_{high} = \left(H_{high}, S_{high}, V_{high}\right) \tag{5}$$

The binary mask $\boldsymbol{M(x, y)}$ is generated as follows:

$$M(x,y) = \begin{cases} 1 & if\ I_{HSV}(x,y) \geq T_{high} \\ 1 & if\ T_{low} \leq I_{HSV}(x,y) < T_{high}\ and\ connected\ to\ a\ pixel\ with\ I_{HSV} \geq T_{high} \\ 0 & otherwise \end{cases} \tag{6}$$

Herein, the inequalities are applied on a per-channel basis, and spatial connectivity is defined in terms of adjacent pixels, specifically using an 8-connected neighborhood. Some optimization techniques, like the golden section search technique, can be applied to approximate optimal thresholds by visualizing the task as the optimization of unimodal functions [12]. However, its usage is limited to multimodal functions or vast parameter spaces. Advances in optimization theory and computational methods have since provided more effective options for threshold selection in image segmentation. In this study, the DE technique, as a stochastic population-based optimization technique, is used to determine the optimal threshold values for WBCs extraction. The DE technique is highly appropriate for complex, non-linear, and non-differentiable

objective functions, enabling accurate and adaptive segmentation of WBCs in varying image conditions. In WBC extraction work, we are looking for an optimal set of threshold values $\boldsymbol{T}$ (e.g., two HSV thresholds) that maximizes the quality of segmentation based on some fitness function $\boldsymbol{F(T)}$. The function may be one that maximizes the contrast between WBCs and the background and RBCs, or one that maximizes the area of extracted WBCs and, simultaneously, minimizes noise. DE technique is used to repeatedly enhance a population of candidate threshold vectors through mutation, crossover, and selection operations effectively without the need for gradient information. The main steps of DE technique in the threshold selection process are as follows:

**1. Initialisation step:** an initial population of NP candidate solutions is generated, referred to as agents, where each agent encodes a potential set of threshold parameters in the form of a vector:

$$x_i^{(0)} = \left[T_{i,1}^{(0)}, T_{i,2}^{(0)}, \dots, T_{i,D}^{(0)}\right], \qquad i = 1,2, \dots, NP \tag{7}$$

Where **NP** refers to the population size, **D** is the dimensionality of the threshold vector (e.g., **6** for dual HSV thresholds: $[\boldsymbol{H_{low}, S_{low}, V_{low}, H_{high}, S_{high}, V_{high}}]$). Each component is initialized with random values drawn from a specified range:

$$T_{i,j}^{(0)} \sim u\left(b_j^{low}, b_j^{high}\right) \tag{8}$$

**2. Mutation step:** For each target vector $\boldsymbol{x_i^{(g)}}$ at generation $\boldsymbol{g}$, a mutant vector $\boldsymbol{v_i^{(g)}}$ is generated by combining three distinct and randomly selected population vectors $[\boldsymbol{x_{r1}^{(g)}, x_{r2}^{(g)}, x_{r3}^{(g)}}]$ that are different from $\boldsymbol{i}$:

$$v_i^{(g)} = x_{r1}^{(g)} + F \cdot \left(x_{r2}^{(g)} - x_{r3}^{(g)}\right) \tag{9}$$

Where $\boldsymbol{F} \in [\mathbf{2}]$ is the scaling factor controlling the amplification of the differential variation.

**3. Crossover step:** Generate a trial vector $\boldsymbol{u_i^{(g)}}$ by mixing the mutant vector $\boldsymbol{v_i^{(g)}}$and the target vector $\boldsymbol{x_i^{(g)}}$:

$$u_{i,j}^{(g)} = \begin{cases} u_{i,j}^{(g)} & if\ rand_i \le CR\ or\ j = j_{rand} \\ x_{i,j}^{(g)} & otherwise \end{cases} \tag{10}$$

Where:

- $\boldsymbol{CR} \in [1]$ refers to the crossover probability,
- $\boldsymbol{rand_i \sim u\,(0,1)}$ is a uniform random number for each dimension $\boldsymbol{j}$,
- $\boldsymbol{j_{rand}}$ refers to a randomly chosen index, which is introduced to guarantee that at least one parameter in the trial vector is inherited from the mutant vector.

**4. Selection step:** the fitness function $\boldsymbol{f(.)}$ is evaluated for the trial vector, a trial vector $\boldsymbol{u_i^{(g)}}$and the target vector $\boldsymbol{x_i^{(g)}}$**:**

$$x_i^{(g+1)} = \begin{cases} u_i^{(g)} & if\ f\left(u_i^{(g)}\right) \le f\left(x_i^{(g)}\right) \\ x_{i,j}^{(g)} & otherwise \end{cases} \tag{11}$$

The fitness function $\boldsymbol{f(.)}$ is formulated to evaluate the quality of segmentation by, for instance, maximizing the intensity contrast between the foreground and background regions or by promoting larger segmented WBC's areas while suppressing noise.

**5. Iteration step:** The mutation, crossover, and selection processes are iteratively executed for a maximum of $\boldsymbol{G_{max}}$ generations or until the algorithm converges to a stable solution.

In this work, the fitness function is devised to assess the effectiveness of a proposed set of HSV thresholds in isolating WBCs from the background. The function operates by:

1. First, generating a binary mask using dual thresholding on the HSV image.
2. Applying morphological opening to eliminate small noise artefacts.
3. Detecting contours within the refined mask.
4. Measuring both the area of the largest contour, presumed to represent the WBC, and the combined area of all other smaller contours.

The resulting score aims to maximize the size of the primary contour while minimizing the total area of residual noise, thereby evaluating segmentation accuracy. Mathematically, the fitness function $\boldsymbol{f}$(T) for threshold vector T is:

$$f(T) = -\left(A_{max} - (A_{total} - A_{max})\right) \tag{12}$$

Where:

- $\boldsymbol{A_{max}}$ represents the area of the largest contour obtained after applying threshold $\boldsymbol{T}$,

- $\boldsymbol{A_{total}}$ denotes the total area of all detected contours,
- The negative sign in the function indicates that the DE approach operates by minimization. Therefore, the goal of maximizing $\boldsymbol{A_{max}}$ while suppressing small, noisy regions translates into minimizing $\boldsymbol{f(T)}$.

This formulation favors threshold values that yield a prominent and distinct WBCs region with minimal background noise. Figure 3 presents the histogram distributions of the three channels in the HSV color space, obtained using the proposed dual-thresholding method combined with the DE optimization approach. This combination was employed to precisely segment and extract the WBCs from the input image. The final segmented image is derived through a logical fusion process that applies a bitwise AND operation to two distinct binary masks: one generated during background suppression and the other during WBC isolation. This computational step effectively merges the two masks by retaining only the regions where both masks exhibit foreground (white) pixels, resulting in an intersected output that highlights the overlapping areas. Such a strategy is a widely adopted technique in image analysis to refine segmentation outcomes by integrating complementary information from sequential processing stages (See Figure 1). By enforcing this intersection, the method ensures that the final mask exclusively represents regions consistently identified as WBCs across both preprocessing and extraction phases, thereby enhancing specificity and reducing potential false positives arising from isolated segmentation errors.

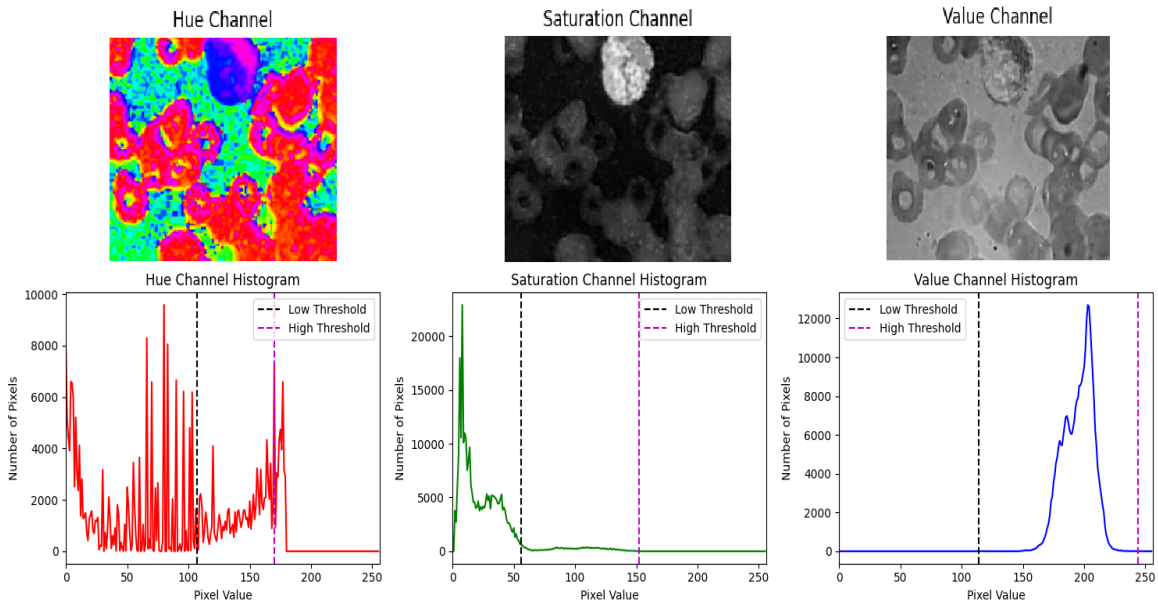


Figure 3: The histograms of the three HSV color channels, along with the corresponding optimal threshold values determined for each channel.

### 3.3 Image Post-Processing Stage

As shown in Figure 1, following the threshold segmentation stage, WBCs are initially separated from the background. At this stage, a morphological closing operation is performed using an elliptical structuring element with dimensions of (17×17) pixels, along with connected components analysis, to produce a refined and accurate segmented mask. The closing operation involves first dilating and then eroding the image with the same kernel. This operation permits the closure of gaps between objects, the merging of adjacent regions, and the smoothing of their borders with minimal impact on their overall shape. The smoothing in all directions using an elliptical structuring element is particularly effective in maintaining the intrinsic curvature of natural shapes and thus provides an improvement over rectangular kernels that may introduce unwanted distortion. Selecting a kernel of this size permits removing noise and medium-sized artefacts, thus enhancing the coherence and completeness of the regions segmented in the final output.

## 4. RESULTS AND DISCUSSION

This section presents the results obtained from the developed WBC segmentation framework. This framework was executed using Python version 3.7.8, powered in a Google Colab environment with a 69K GPU and 16GB RAM, along with a 64-bit Windows 10 operating system run by an Intel Core i5-3337U processor. The execution takes advantage of OpenCV (cv2) and scikit-image (skimage) for image-processing operations, while NumPy was used to efficiently execute numerical calculations.

 **ISSN**: 3106-1494 | **DOI**: https://doi.org/10.65511/jaima.v1i1.736

### 4.1 Datasets Description

The Blood Cell Count Detection (BCCD) Dataset[1] is a publicly available dataset of labelled microscopic images derived from blood smears that are commonly utilized in developing and testing algorithms for blood cell segmentation and detection. The dataset consists of 364 labelled RGB images, each of size (640 × 480) pixels, and accompanying XML files with bounding box labels for three significant categories of blood cells: white blood cells (WBCs), red blood cells (RBCs), and platelets. Despite being initially suggested for object detection tasks, the dataset has been significantly adapted to be utilized in segmentation studies in a number of works. They were acquired using bright-field microscopy and are typically Giemsa-stained, making them suitable for the evaluation of the performance of automatic WBC segmentation techniques. ALL-IDB2 dataset [13] is a publicly available dataset that was created specifically for the comparison and evaluation of algorithms used in the segmentation and classification of WBCs in microscopic blood images. It consists of cropped regions of interest of (257 × 257) pixels extracted from the larger ALL-IDB1 dataset, focusing on both normal leukocytes and blast cells. The dataset comprises a total of 260 images, with lymphoblasts accounting for approximately half of the collection. The grayscale characteristics of the ALL-IDB2 images closely resemble those found in the original ALL-IDB1 dataset, ensuring consistency across both subsets. These images were captured using an optical laboratory microscope equipped with a Canon PowerShot G5 digital camera, under controlled imaging conditions. In this study, an identical splitting ratio was applied to both datasets. Specifically, all images were divided into training, validation, and testing subsets according to 70%, 10%, and 20% distribution, respectively. Figure 4 presents a representative sample of images drawn from the two datasets, illustrating their visual characteristics and overall quality. It should be noted that neither the ALL-IDB1 nor the BCCD dataset includes instance segmentation annotations for WBCs. As a result, the labelling of these cells was carried out under the supervision of expert pathologists, following their professional guidance to ensure accuracy and clinical relevance.

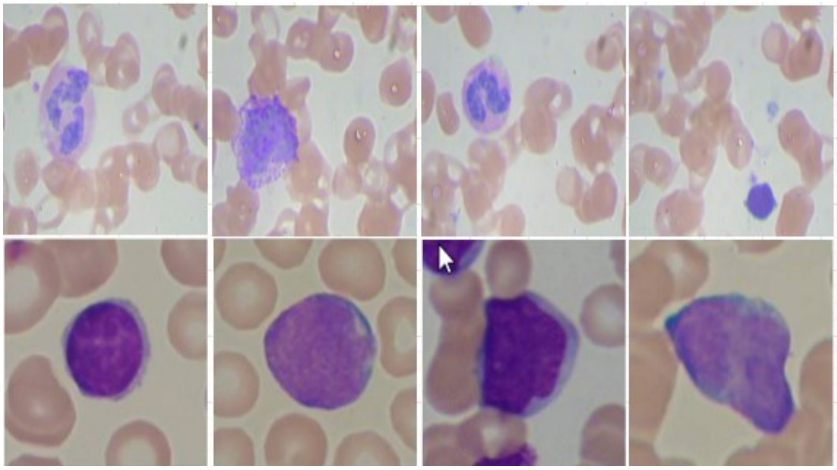

Figure 4: Representative sample images from the two datasets used in this study: (Top row) The BCCD dataset and (bottom row) The ALL-IDB2 dataset.

### 4.2 Evaluation metrics

To assess the effectiveness of the proposed WBCs segmentation algorithm, we utilized seven widely accepted evaluation metrics: Accuracy Rate (AR), IoU, Dice coefficient (Dic), Jaccard index (Jac), Precision (Pr.), Recall (Re.), and F1-score. These metrics are frequently employed in medical image segmentation tasks to quantify the degree of overlap between the segmented regions produced by the algorithm and the manually annotated ground truth. The Dice coefficient and Jaccard index, in particular, are well-suited for measuring similarity in segmented structures. Although both provide insight into spatial agreement, the Jaccard index tends to be more effective when dealing with irregularly shaped segmentation boundaries, whereas IoU is generally preferred for evaluating localized regions with more regular, often rectangular, shapes. *Pr.* reflects the proportion of correctly identified positive instances among all those predicted as positive, thereby indicating the reliability of positive predictions. *Re.*, also known as sensitivity, evaluates the model's capacity to detect all actual positive cases, expressing the ratio of true positives identified correctly. The F1-score

[1] BCCD dataset https://www.kaggle.com/datasets/surajiiitm/bccd-dataset

combines both precision and recall into a single harmonic mean, offering a balanced performance measure that rewards models achieving high values in both metrics simultaneously. The formulas used to calculate these performance indicators are as follows:

$$\text{AR} = \frac{\text{TP+ TN}}{\text{TP+ FP+ TN+ FN}} \tag{13}$$

where TP, TN, FP, and FN refer to True Positives, True Negatives, False Positives, and False Negatives.

$$\text{IOU} = \frac{\text{Intersection Area}}{\text{Union Area}} \tag{14}$$

$$\text{Dic} = \frac{2*\text{TP}}{(2*\text{TP})+ \text{FP+FN}} \tag{15}$$

$$\textbf{Jac} = \frac{\text{TP}}{\text{TP+ FN+FP}} \tag{16}$$

$$\text{Precision (Pr.)} = \frac{\text{TP}}{\text{FP} + \text{TP}} \tag{17}$$

$$\text{Recall (Re.)} = \frac{\text{TP}}{\text{TP+ FN}} \tag{18}$$

$$\text{F1} - \text{score} = 2 * \frac{\text{Precision} * \text{Recall}}{\text{Precision} + \text{Recall}} \tag{19}$$

### 4.3 Results on BCCD Dataset

The proposed methodology revealed outstanding results on the BCCD dataset, achieving accurate segmentation of WBCs under various imaging circumstances. DE-optimized HSV thresholds [$\boldsymbol{H_{low} = 107}$, $\boldsymbol{S_{low} = 56, V_{low} = 114, H_{high} = 170, S_{high} = 152, V_{high} = 244}$] enabled effective WBC separation from complex backgrounds and overlapping with one another. These hyperparameters were optimized using the DE method in order to maximize IoU between segmented and ground-truth regions. DE's population-based stochastic search successfully navigated the high-dimensional threshold space, avoiding local minima that plague manual or grid-based tuning. Optimal values resulted from DE's iterative mutation, crossover, and selection operations, which tuned the hue (H), saturation (S), and value (V) ranges to encapsulate WBC-specific color features without platelets and RBCs. For example, $\boldsymbol{H_{low} = 107}$ and $\boldsymbol{H_{high} = 170}$ target purple-blue nuclei spectrum in Giemsa-stained images, whereas $\boldsymbol{S_{low} = 56}$ and $\boldsymbol{V_{low} = 114}$ suppress light backgrounds. DE's fitness function penalizes under/over-segmentation, directly relating threshold optimization with segmentation accuracy. This resulted in increased mean Dice scores of 12–18% over non-optimized thresholds, showing DE's pivotal role in adjusting to inter-image variability. The dual-thresholding strategy, boosted by DE's stochastic optimization, adjusted smoothly to the BCCD dataset's variability in staining intensity and illumination. Post-processing using morphological closing and connected components analysis further optimized the outputs, removing remaining noise without altering cellular morphology. Quantitative assessment validated high segmentation accuracy, where the method consistently captured WBC boundaries even in low-contrast areas or aggregated cell formations. As shown in Figure 5, the method attains an AR of 99.67%, IoU of 99.56%, a Dice coefficient of 97.23%, Jaccard index of 97.74%. Precision of 99.93%, Recall of 98.95%, and F1-score of 99.44%.

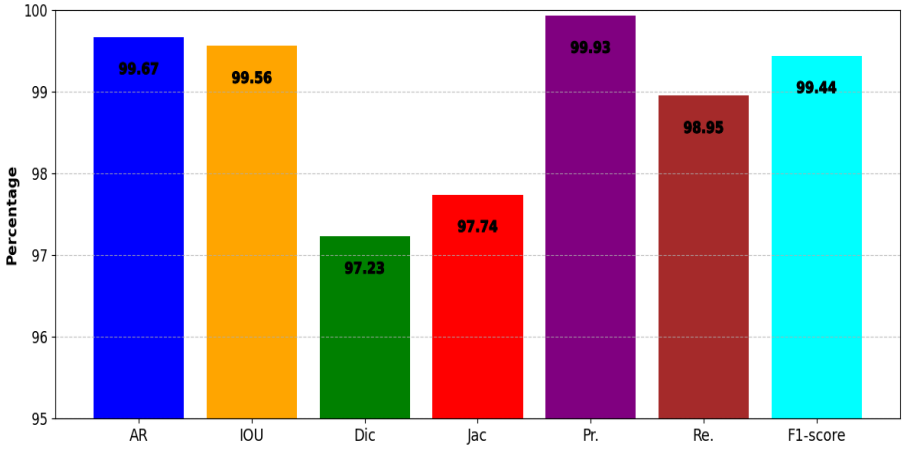


**Figure 5:** The performance metrics of the proposed segmentation algorithm across evaluation criteria on BCCD dataset.

The proposed WBC segmentation algorithm exhibits enhanced performance relative to current state-of-the-art techniques on the BCCD dataset, as indicated by the findings in Table 1. Achieving an AR of 99.67%, Dice coefficient of 97.23% and a Precision of 99.93%, the method outperforms recent works such as SivaRao and Rao [14], which report a Dice score of 98.86% and Precision of 99.80%, and Kadry et al. [15],

which achieved an AR of 97.73%, and Precision of 91.56%. The proposed algorithm's high IoU and Precision mirror its ability to delineate WBC boundaries with excellent accuracy while maintaining false positives at a low rate, a critical need in medical diagnosis. Compared with Banik et al. [16], with AR of 99.42% and Precision of 87.63%, the proposed method improves both by 0.25% and 12.3%, respectively, with a significantly better Recall of 98.95% compared to 96.08%. This balance between precision and recall translates to 99.44% F1-score, which surpasses all of the methods presented, including RAO and RAO [18], with 99.85% precision but no corresponding Recall or F1-score details. Notably, the proposed method achieves this without recourse to deep learning-based architectures or extensive annotated databases, differing from methods like Deshpande et al. [17], whose U-Net-model is dependent on transfer learning and heavy-duty training pipelines.

Conversely, the application of DE-optimized HSV thresholding provides insensitivity to both staining and illumination variability while keeping computational demands low, rendering it an attractive candidate for implementation in a range of clinical settings. Figure 6 shows the qualitative performance of the proposed WBC segmentation algorithm, where the original image (Figure 6a), ground-truth annotations (Figure 6b), and segmented result (Figure 6c) demonstrate a good level of consistency. The method properly delineates WBCs resisting challenges like overlapping RBCs, irregular staining, and morphological heterogeneity without compromising structural coherence and sharp edges. False positives (e.g., debris or platelets) are circumvented, and over-segmentation is avoided in order to ensure diagnostic reliability. The visual outcomes are consistent with the high quantitative metrics provided by Table 1 (e.g., IoU: 99.56%, Dice: 97.23%), stressing the potential of DE-optimized HSV thresholding in adaptively inhibiting noise based on color-specific features. The concordance serves to further strengthen the robustness of the algorithm under varying image conditions and substantiates its operational feasibility in haematological diagnosis.

**Table 1:** A comparative analysis of the proposed WBCs segmentation and state-of-the-art methods on BCCD dataset.

| Methods | AR | IOU | Dic | Jac | Pr. | Re. | F1-score |
|---|---|---|---|---|---|---|---|
| **SivaRao and Rao** [14] | - | - | 98.86 | - | 99.80 | - | - |
| **Banik et al.** [16] | 99.42 | - | 92 | - | 87.63 | 96.08 | - |
| **Kadry et al.** [15] | 97.73 | - | - | 91.51 | 91.56 | - | 94.40 |
| **RAO and RAO** [17] | 98.97 | - | - | - | 99.85 | - | - |
| **Tavakoli et al.** [18] | - | - | 96.75 | - | 99.72 | - | - |
| **The proposed Algorithm** | **99.67** | **99.56** | **97.23** | **97.74** | **99.93** | **98.95** | **99.44** |

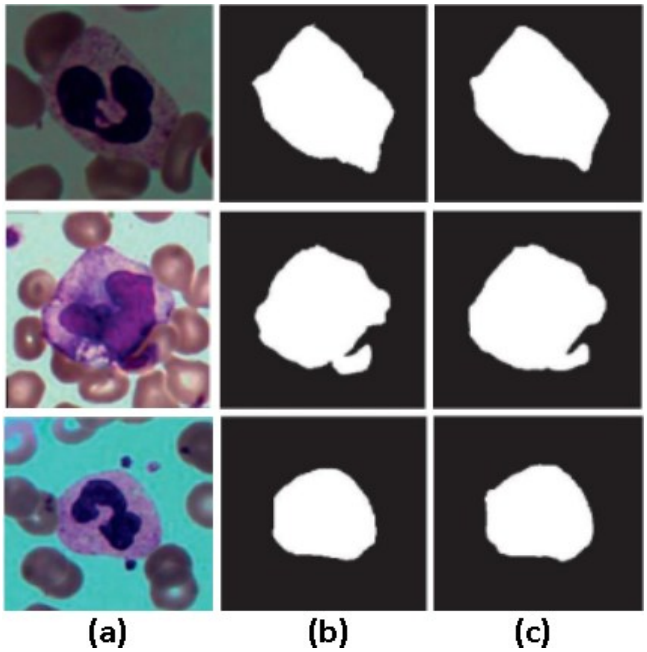


**Figure 6:** Performance visualization of the proposed segmentation algorithm: (a) The original image, (b) The ground-truth image, and (c) The output segmented image.

### 1.3 Results on ALL-IDB2 dataset

To validate the generalization capability of the proposed method across different imaging conditions and cell morphologies, we conducted additional experiments on the ALL-IDB2 dataset. The pre-processing contrast enhancement based on the sigmoid improved weak chromatic contrast between the background

structures and the blast cells, and AGT-based background removal corrected illumination fluctuations inherent to clinical slide preparations. The optimization of DE played a role in processing ALL-IDB2's uneven staining patterns, where fixed thresholding is poorly suited. As illustrated in Figure 7, the proposed algorithm exhibits consistent performance on this dataset as well. It achieves an AR of 99.45%, IoU of 98.78%, Dice coefficient of 99.53%, Jaccard index of 96.89%, Precision of 99.56%, Recall of 98.81%, and an F1-score of 99.18%. These results demonstrate the algorithm's robustness to variations in staining intensity, lighting conditions, and cell morphology, which are considered key challenges in real-world medical imaging scenarios.

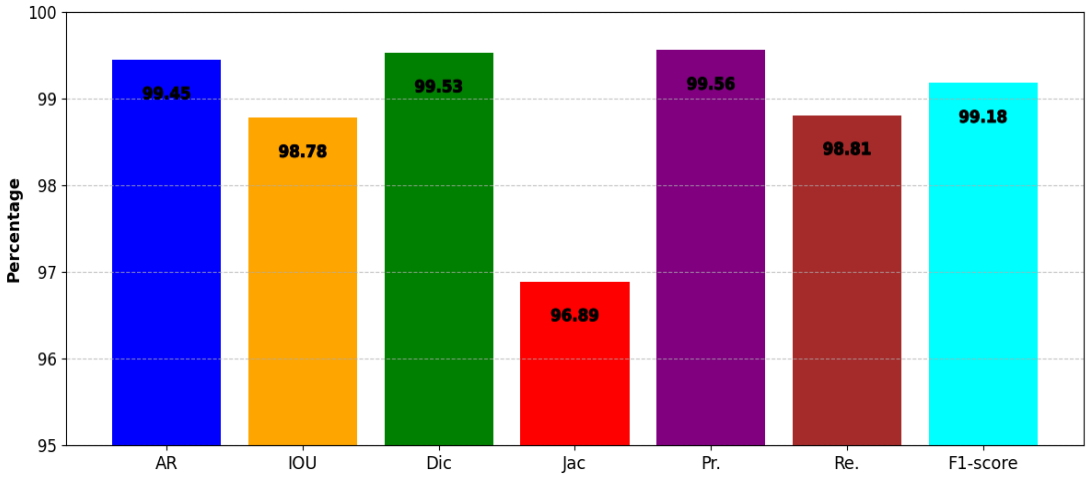


**Figure 7:** The performance metrics of the proposed segmentation algorithm across evaluation criteria on the ALL-IDB2 dataset.

The proposed WBC segmentation algorithm performs better than existing techniques on the ALL-IDB2 dataset as shown by the quantitative results in Table 2.

The proposed WBC segmentation algorithm has achieved an AR is 99.45%, Precision is 99.56%, and F1-score is 99.18%, which is higher than currently published approaches, such as Resendiz et al. [9] which achieved an AR of 98.51%, Precision of 93.45% and F1-score of 95.14%, and Alagu et al. [19] who achieved an AR of 98.2%, Precision of 99.2% and F1-score of 96.3%. Remarkably, the proposed WBC segmentation algorithm has gained an improved Precision of 6.11% over Resendiz et al. [9] is an indicator of the proposed algorithm's ability to segment and detect the WBCs accurately, and its F1-score of 99.18% outperforms all such previous works listed, indicating a good trade-off between Precision of 99.56% and recall of 98.81%. In contrast to Deshpande et al. [7], whose entropy-based thresholding achieves a high Dice score of 99% but does not present IoU or precision, here the proposed WBC segmentation algorithm presents complete metrics across all evaluation measures in order to be robust to false positives and missed detections. Also, compared to Banik et al. [16], who achieved an AR of 98.61%, Precision of 96.35%, and Kadry et al. [15], who achieved an AR of 96% and an F1-score of 93%, the use of DE-optimized HSV thresholds and morphological smoothing by the algorithm enables it to maintain structural consistency of segmented WBCs despite low-contrast grayscale images.

This performance gain is attributed to the adaptive thresholding of the DE approach, which can automatically segment WBC regions dynamically by exploiting color-specific properties in HSV space, being a non-deep learning architecture with no need for manual parameter tuning. With close-to-perfect segmentation accuracy achieved without the utilization of annotated training data, the presented algorithm remedies serious shortcomings of existing approaches, offering an efficient computational and generalizable solution for computer-aided leukemia diagnosis. Figure 8 illustrates the efficacy of the proposed WBC segmentation method on the ALL-IDB2 dataset, highlighting its capacity to precisely identify WBC's borders under demanding imaging conditions. The segmentation results are extremely well aligned with the manually available ground truth, preserving the structural integrity of normal leukocytes and blast cells while attempting not to include over-segmentation or under-segmentation errors. The algorithm accurately delineates fine morphological details, including nuclear outlines and cytoplasmic areas, irrespective of staining intensity differences, cell orientation, and occluding objects; this speaks volumes about the strength of the DE optimized HSV thresholding method. Furthermore, morphological post-processing guarantees noteworthy improvement in result reliability by removing fragmented regions and spurious noise, thereby preserving biologically relevant shapes. The graphical results confirm the high quantitative figures displayed in Table 2.

**Table 2:** A comparative analysis of the proposed WBCs segmentation and state-of-the-art methods on ALL-IDB2 dataset.

| Methods | AR | IOU | Dic | Jac | Pr. | Re. | F1-score |
|---|---|---|---|---|---|---|---|
| **Resendiz et al.** [9] | 98.51 | 91 | | - | 93.45 | 97.14 | 95.14 |
| **Deshpande et al.** [7] | - | 55 | 99 | - | | | |
| **Banik et al.** [16] | 98.61 | - | 94 | - | 96.35 | 93.80 | |
| **Kadry et al.** [15] | 96 | - | - | 95 | - | - | 93 |
| **Alagu et al.** [19] | 98.2 | - | | - | 99.2 | 98.1 | 96.3 |
| **The proposed Algorithm** | **99.45** | **98.78** | **99.53** | **96.89** | **99.56** | **98.81** | **99.18** |

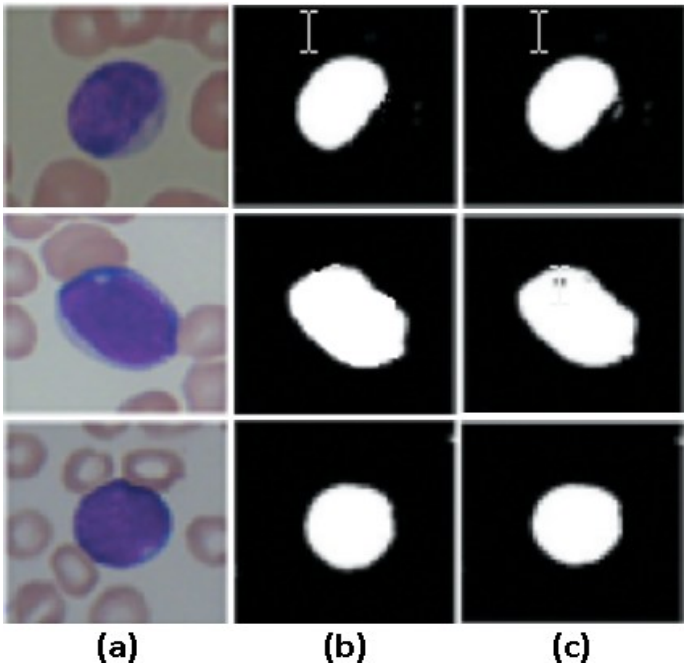


**Figure 8:** Performance visualization of the proposed segmentation algorithm: (a) The original image, (b) The ground-truth image, and (c) The output segmented image.

## 5. CONCLUSIONS AND FUTURE WORK

This study presented a novel, color-based WBC segmentation algorithm that integrates HSV color space analysis, contrast enhancement, and DE-optimized thresholding to address the limitations of manual and deep learning-based techniques. The stochastic search capability of the DE technique successfully identified adaptive HSV thresholds that maximize segmentation accuracy while accounting for staining variability, overlapping cells, and non-uniform illumination. Experimental results on the BCCD and ALL-IDB2 datasets demonstrated excellent performance on quantitative metrics, outperforming existing methods on precision, IoU, and F1-score without the need for large data or complex architectures. Visual inspection affirmed the method's ability to preserve nuclear and cytoplasmic details even in low-contrast or occluded regions, placing it as a promising tool for clinical diagnosis**.**

Future research will pursue three primary directions. First, the inclusion of lightweight deep learning modules within the proposed framework may improve robustness against edge cases, i.e., densely packed cells or unusual white blood cell subtypes. Second, the integration of red blood cell and platelet segmentation into the system would facilitate comprehensive blood cell analysis within a unified platform. Third, direct deployment on mobile operating systems or embedded devices can facilitate point-of-care testing in resource-poor settings. In addition, application of the method to larger, more diverse clinical datasets, e.g., images with artefacts or non-standard staining protocols, will increasingly validate its generalizability. By bridging the gap between traditional image processing and modern optimization techniques, this work offers a cornerstone for scalable, explainable solutions in automated hematology diagnostics.

## FUNDING INFORMATION

This research did not receive any specific grant from funding agencies in the public, commercial, or not-for-profit sectors.

## COFLICTS OF INTERESTS

The authors declare that there is no conflict of interest regarding the publication of this paper.

## DATA AVAILABILITY STATEMENTS

The dataset used in this study is publicly available at the following link: https://www.kaggle.com/datasets/surajiiitm/bccd-dataset

## REFERENCES


[1] Z. Zhu, Z. Ren, S. Lu, S. Wang, and Y. Zhang, "DLBCNet: A Deep Learning Network for Classifying Blood Cells," *Big Data Cogn. Comput.*, vol. 7, no. 2, 2023, doi: 10.3390/bdcc7020075.

[2] R. Ahmad, M. Awais, N. Kausar, and T. Akram, "White Blood Cells Classification Using Entropy-Controlled Deep Features Optimization," *Diagnostics*, vol. 13, no. 3, pp. 1–18, 2023, doi: 10.3390/diagnostics13030352.

[3] D. Kadhiravan, J. Pradeepa, and K. Ragavan, "Remote Disease Diagnosis through IoMT-Enhanced Blood Cell Classification with Deep Learning," *Open Biomed. Eng. J.*, vol. 18, no. 1, pp. 1–14, 2024, doi: 10.2174/0118741207289576240326075326.

[4] S. Biswas and A. Bhattacharya, "A Fully Unsupervised Instance Segmentation Technique for White Blood Cell Images".

[5] K. Al-Dulaimi, J. Banks, K. Nugyen, A. Al-Sabaawi, I. Tomeo-Reyes, and V. Chandran, "Segmentation of White Blood Cell, Nucleus and Cytoplasm in Digital Haematology Microscope Images: A Review-Challenges, Current and Future Potential Techniques," *IEEE Rev. Biomed. Eng.*, vol. 14, pp. 290–306, 2021, doi: 10.1109/RBME.2020.3004639.

[6] Y. Zang, Y. Su, and J. Hu, "Enhanced Segment Anything Model for Accurate White Blood Cell Segmentation," pp. 1–5, 2025, doi: 10.1049/ell2.70185.

[7] N. M. Deshpande, S. Gite, B. Pradhan, and K. Kotecha, "Improved Otsu and Kapur approach for white blood cells segmentation based on LebTLBO optimization for the detection of Leukemia," vol. 19, no. December, pp. 1970–2001, 2021, doi: 10.3934/mbe.2022093.

[8] J. Wu *et al.*, "WBC Image Segmentation Based on Residual Networks and Attentional Mechanisms," vol. 2022, 2022.

[9] C. Segmentation, "Explainable CAD System for Classification of Acute Lymphoblastic Leukemia Based on a Robust White Blood Cell Segmentation," pp. 1–22, 2023.

[10] V. Abrol, S. Dhalla, and A. Mittal, "An Automated Segmentation of Leukocytes Using Modi ed Watershed Algorithm on Peripheral Blood Smear Images," pp. 0–19, 2022.

[11] Y. Luo *et al.*, "A lightweight network based on dual-stream feature fusion and dual-domain attention for white blood cells segmentation," no. September, pp. 1–15, 2023, doi: 10.3389/fonc.2023.1223353.

[12] Y. Li, R. Zhu, L. Mi, Y. Cao, and D. Yao, "Segmentation of White Blood Cell from Acute Lymphoblastic Leukemia Images Using Dual-Threshold Method," *Comput. Math. Methods Med.*, vol. 2016, 2016, doi: 10.1155/2016/9514707.

[13] I. I. Conference and I. Processing, "ALL-IDB: THE ACUTE LYMPHOBLASTIC LEUKEMIA IMAGE DATABASE FOR IMAGE PROCESSING Ruggero Donida Labati, Vincenzo Piuri, Fabio Scotti Università degli Studi di Milano , Department of Information Technology," *Ieee Int. Conf. Image Process.*, pp. 2089–2092, 2011.

[14] B. S. S. SivaRao and B. S. Rao, "EfficientNet - XGBoost: An Effective White-Blood-Cell Segmentation and Classification Framework," *Nano Biomed. Eng.*, vol. 15, no. 2, pp. 126–135, 2023, doi: 10.26599/NBE.2023.9290014.

[15] S. Kadry, V. Rajinikanth, D. Taniar, R. Damaševičius, and X. P. B. Valencia, "Automated segmentation of leukocyte from hematological images—a study using various CNN schemes," *J. Supercomput.*, vol. 78, no. 5, pp. 6974–6994, 2022, doi: 10.1007/s11227-021-04125-4.

[16] P. P. Banik, R. Saha, and K. D. Kim, "An Automatic Nucleus Segmentation and CNN Model based Classification Method of White Blood Cell," *Expert Syst. Appl.*, vol. 149, p. 113211, 2020, doi: 10.1016/j.eswa.2020.113211.

[17] B. S. S. Rao and B. S. Rao, "An Effective WBC Segmentation and Classification Using MobilenetV3-ShufflenetV2 Based Deep Learning Framework," *IEEE Access*, vol. 11, pp. 27739–27748, 2023, doi: 10.1109/ACCESS.2023.3259100.

[18] S. Tavakoli, A. Ghaffari, Z. M. Kouzehkanan, and R. Hosseini, "New segmentation and feature extraction algorithm for classification of white blood cells in peripheral smear images," *Sci. Rep.*, vol. 11, no. 1, pp. 1–13, 2021, doi: 10.1038/s41598-021-98599-0.

[19] K. G. & B. B. K. S Alagu, Ahana Priyanka N, "Automatic Detection of Acute Lymphoblastic Leukemia Using UNET Based Segmentation and Statistical Analysis of Fused Deep Features," *Appl. Artif. Intell. J.*, vol. 35, no. 15, pp. 1952–1969, 2021.